Deblurring Images via Dark Channel Prior

Jinshan Pan [ID], Deqing Sun, *Member, IEEE*, Hanspeter Pfister, and
Ming-Hsuan Yang [ID], *Senior Member, IEEE*

Abstract—We present an effective blind image deblurring algorithm based on the dark channel prior. The motivation of this work is an interesting observation that the dark channel of blurred images is less sparse. While most patches in a clean image contain some dark pixels, this is not the case when they are averaged with neighboring ones by motion blur. This change in sparsity of the dark channel pixels is an inherent property of the motion blur process, which we prove mathematically and validate using image data. Enforcing sparsity of the dark channel thus helps blind deblurring in various scenarios such as natural, face, text, and low-illumination images. However, imposing sparsity of the dark channel introduces a non-convex non-linear optimization problem. In this work, we introduce a linear approximation to address this issue. Extensive experiments demonstrate that the proposed deblurring algorithm achieves the state-of-the-art results on natural images and performs favorably against methods designed for specific scenarios. In addition, we show that the proposed method can be applied to image dehazing.

Index Terms—Image deblurring, dark channel prior, non-uniform deblurring, convolution, linear approximation

✦

1 INTRODUCTION

BLIND image deblurring aims to recover a blur kernel and a sharp latent image from a blurred image. It is a classical problem [1] in computer vision and image processing, which has become increasingly important as more photos are taken using hand-held devices where camera shake is often inevitable and the resulting motion blur is undesirable. As captured moments are ephemeral and scenes are difficult to reproduce, it is of great interest to remove motion blur and restore higher-quality images.

When the blur is uniform and spatially invariant, the image formation can be modeled by the linear convolution

$$B = I \otimes k + n, \qquad (1)$$

where B, I, k, and n denote the blurred image, latent image, blur kernel, and noise, respectively. In addition, $\otimes$ is the convolution operator. As only B is available, we need to recover both I and k simultaneously. This problem is ill-posed as many different pairs of I and k render the same B, e.g., blurred images and delta blur kernels.

To make the blind deblurring problem well-posed, existing methods exploit statistical priors of blur kernels, latent images, or both [2], [3], [4], [5], [6], [7], [8]. For example, numerous methods [2], [3], [5], [9] assume sparsity of image gradients, which has been widely used in low-level vision tasks including denoising, stereo, and optical flow. Levin et al. [9] show that deblurring methods based on this prior tend to favor blurry images over original clear ones, especially for algorithms formulated within the maximum a posterior (MAP) framework. To remedy this problem, an edge selection step [10], [11] is often used in the MAP framework for effective image deblurring. Various natural image priors have also been introduced in deblurring methods to favor clean images over blurred ones, e.g., normalized sparsity prior [4], L_0-regularized prior [8], and internal patch recurrence [12]. However, the models developed for natural images do not generalize well to other specific scenarios such as face [13], text [6], [14], [15], or low-illumination [16] images.

We present an effective algorithm that can be applied to numerous scenarios including natural, face, text, and low-illumination images. Our work is motivated by an interesting observation on the blur process: dark channels (smallest pixel values in a local neighborhood) of blurred images are less dark. Intuitively, when a dark pixel is averaged with neighboring high-intensity ones during the blur process, the intensity value increases. We show mathematically and empirically that this generic property of dark channel pixels with the blur process holds for many images. This motivates us to propose an L_0-regularization term to minimize the dark channel pixels of the recovered image. The proposed regularization term facilitates recovering clean over blurred images in the restoration process.

Optimizing the new L_0-regularized term on dark channel pixels is challenging. The L_0 norm is non-convex and the optimization problem involves a non-linear minimum operation. We propose an approximate linear operator based on look-up tables for the minimum operator, and solve the linearized L_0 minimization problem by a half-quadratic splitting method. The proposed algorithm converges fast in practice and can be easily extended to non-uniform deblurring tasks.

- *J. Pan is with the School of Computer Science and Engineering, Nanjing University of Science and Technology, Nanjing 210094, China. E-mail: sdluran@gmail.com.*
- *D. Sun is with NVIDIA, Westford, MA 01886. E-mail: deqings@nvidia.com.*
- *H. Pfister is with Harvard University, Cambridge, MA 02138. E-mail: pfister@seas.harvard.edu.*
- *M.-H. Yang is with the School of Engineering, University of California, Merced, CA 95344. E-mail: mhyang@ucmerced.edu.*

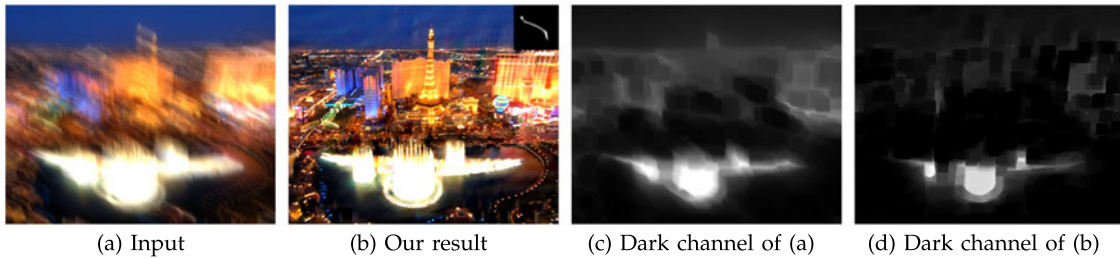| (a) Input | (b) Our result | (c) Dark channel of (a) | (d) Dark channel of (b) |

Fig. 1. Deblurred result on a challenging low-light image. The motion blur process makes the dark channel pixels of the blurred image less sparse (c). Enforcing sparsity on the dark channel pixels of the recovered image facilitates restoring a clean image rather than a blurred one.

Fig. 1 shows a challenging example and results generated by the proposed algorithm.

The main contributions of this work are summarized as follows. First, we show mathematically that the blur (convolution) operation increases the values of the dark channel pixels. Second, we empirically confirm our analysis using a dataset of 3,200 clean and blurred image pairs. Third, we introduce an L_0-regularization term to enforce sparsity on the dark channel pixels of latent images and develop an efficient optimization scheme. Fourth, we demonstrate that the proposed algorithm achieves the state-of-the-art results on the natural image deblurring benchmark datasets [9], [17], [18], and performs favorably on specific deblurring tasks including text, face, and low-illumination images, which are not handled well by most deblurring methods designed for natural images. Finally, the proposed algorithm can be applied to non-uniform deblurring.

This proposed algorithm is extended from our preliminary work [19] with the following differences. First, we present more detailed analysis and discussion of the dark channel prior in image deblurring. Second, we further analyze the limitations of the proposed method and confirm the analysis with empirical results. Third, we carry out sensitivity analysis of the parameters in the proposed model and show that the proposed method is robust within a wide range of parameter values. Fourth, we extend the proposed sparsity of dark channel prior to effective image dehazing.

2 RELATED WORK

The recent years have witnessed significant advances in single image deblurring [17], [20] due to effective statistical priors of natural scenes and extraction of salient edges for kernel estimation [3], [4], [5], [7], [8], [10], [11]. In this section, we discuss the methods most related to this work within proper contexts.

Fergus et al. [3] use a mixture of Gaussians to learn an image gradient prior within the variational Bayesian framework. In [9] Levin et al. show that the variational Bayesian inference method [3] is able to avoid trivial solutions while naive MAP based methods may not. However, the variational Bayesian approach is computationally expensive, and efficient methods require certain approximations [5].

Efficient methods based on MAP formulations have been developed with different likelihood functions and image priors [4], [7], [8], [21], [22], [23], [24], [25]. In particular, the edge selection methods [10], [11], [26] have been proposed for the MAP based image deblurring approaches [17]. The edge selection step usually requires heuristic filters and thresholds to remove subtle image structures and preserve

sharp edges. However, the assumption that strong edges can be extracted from blurred images may not always hold.

To extract sharp edges for kernel estimation, recent exemplar based methods [13], [18], [27] exploit information contained in both a blurred input and example images from an external dataset. Such methods are able to handle blurred images when only some sharp edges can be extracted. However, querying a large external dataset for similar example images is computationally expensive.

Numerous methods exploit domain-specific statistical properties for deblurring such as text [6], [14], [15], face [13], and low-illumination images [16]. While these domain-specific methods generate better results than generic deblurring algorithms, each application requires specific operations. In this work, we propose an effective algorithm based on the dark channel prior without specific processing steps for different scenarios. In recent years, neural networks have been applied to blind image deblurring [28], [29], [30], [31]. However, it is difficult to synthesize realistic motion blur kernels as the training data for neural networks. Thus, these methods do not perform well on images with complex and large motion blurs.

The dark channel prior has been applied to single image dehazing [32] based on the assumption that the intensity values of dark channel pixels in a haze-free outdoor image are zero. In this work, we make a less restrictive assumption that the intensity values of dark channel pixels of a clear image are sparse instead of zero. More importantly, we show that the proposed method is able to deblur a large variety of images. To enforce the sparsity of the dark channel pixels, we develop a novel optimization scheme for the formulated optimization problem. In addition, we show that the sparsity assumption of the dark channel pixels is effective for image dehazing.

3 CONVOLUTION AND DARK CHANNEL

We first describe the dark channel and its role in image deblurring. For an image I, the dark channel [32] is defined by

$$D(I)(\mathrm{x}) = \min_{\mathrm{y} \in \mathcal{N}(\mathrm{x})} \left(\min_{c \in \{r,g,b\}} I^c(\mathrm{y}) \right), \qquad (2)$$

where x and y denote pixel locations; $\mathcal{N}(\mathrm{x})$ is an image patch centered at x; and I^c is the cth color channel. If I is a gray-scale image, we have $\min_{c \in \{r,g,b\}} I^c(\mathrm{y}) = I(\mathrm{y})$. The dark channel prior is mainly used to describe the minimum value in an image patch. He et al. [32] observe that the dark channel pixel of an outdoor, haze-free image is almost zero. We find that most, although not all, pixel values of the dark channel are zero in a natural image (see Figs. 2a and 2c).

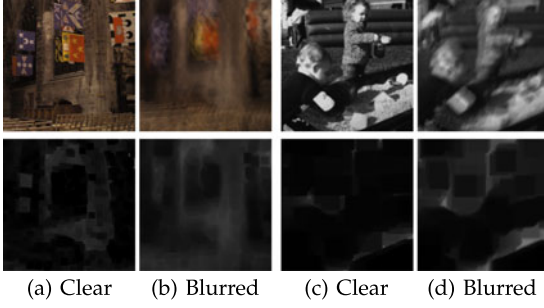(a) Clear   (b) Blurred   (c) Clear   (d) Blurred

Fig. 2. Blurred images have less sparse dark channel pixels than clear ones. Top: Images. Bottom: Corresponding dark channels computed with an image patch of 35×35 pixels. The blur process (convolution) results in a weighted average of pixels in a neighborhood and tends to increase the minimal pixel values.

However, most pixels in the dark channel of blurred images are nonzero, as shown in Figs. 2b and 2d.

To explain why the dark channel pixels of a blurred image are less sparse, we derive some properties of the blur (convolution) operation. For discrete signals (images), convolution is defined as the sum of the product of the two signals after one is reversed and shifted

$$B(\mathrm{x}) = \sum_{\mathrm{z} \in \Omega_k} I\left(\mathrm{x} + \left[\frac{\mathrm{s}}{2}\right] - \mathrm{z}\right)k(\mathrm{z}), \qquad (3)$$

where Ω_k and s denote the domain and size of the blur kernel k, $k(\mathrm{z}) \geq 0$, $\sum_{\mathrm{z} \in \Omega_k} k(\mathrm{z}) = 1$, and $[\cdot]$ denotes the rounding operator. We note that (3) can be regarded as a weighted sum of local pixels in I.

Intuitively, the weighted sum of pixel values in a local neighborhood is larger than the minimum pixel value in the neighborhood, i.e., convolution increases the values of the dark pixels. As such, we have the following proposition.

Proposition 1. *Let $\mathcal{N}(\mathrm{x})$ denote a patch centered at pixel x with size the same as the blur kernel. We have*

$$B(\mathrm{x}) \geq \min_{\mathrm{y} \in \mathcal{N}(\mathrm{x})} I(\mathrm{y}). \qquad (4)$$

Proof. Based on the definition of convolution (3), we have

$$B(\mathrm{x}) = \sum_{\mathrm{z} \in \Omega_k} I\left(\mathrm{x} + \left[\frac{\mathrm{s}}{2}\right] - \mathrm{z}\right)k(\mathrm{z}) \geq \sum_{\mathrm{z} \in \Omega_k} \min_{\mathrm{y} \in \mathcal{N}(\mathrm{x})} I(\mathrm{y})k(\mathrm{z})$$
$$= \min_{\mathrm{y} \in \mathcal{N}(\mathrm{x})} I(\mathrm{y}) \sum_{\mathrm{z} \in \Omega_k} k(\mathrm{z}) = \min_{\mathrm{y} \in \mathcal{N}(\mathrm{x})} I(\mathrm{y}). \qquad \square$$

Note that when x is the dark pixel in its neighborhood, i.e., $I(\mathrm{x}) = \min_{\mathrm{y} \in \mathcal{N}(\mathrm{x})} I(\mathrm{y})$, $B(\mathrm{x}) \geq I(\mathrm{x})$. This means that the intensity values of dark channel pixels in I tend to become larger after the convolution, as shown in Fig. 2.

We use Proposition 1 to derive two properties that describe the changes of dark channel pixels by convolution.

Property 1. *Let $D(B)$ and $D(I)$ denote the dark channel of the blurred and clear images, we have*

$$D(B)(\mathrm{x}) \geq D(I)(\mathrm{x}). \qquad (5)$$

Proof. Let $\mathcal{S}_{\mathcal{N}}$, $\mathcal{S}_{\mathcal{N}^\mathcal{I}}$, and $\mathcal{S}_k$ denote the size of image patches $\mathcal{N}(\mathrm{x})$, $\mathcal{N}^\mathcal{I}(\mathrm{x})$, and blur kernel k. We have $\mathcal{S}_{\mathcal{N}^\mathcal{I}} = \mathcal{S}_{\mathcal{N}} + \mathcal{S}_k$.

According to the definition of dark channel

$$D(B)(\mathrm{x}) = \min_{\mathrm{y} \in \mathcal{N}(\mathrm{x})} B(\mathrm{y})$$
$$= \min_{\mathrm{y} \in \mathcal{N}(\mathrm{x})} \sum_{\mathrm{z} \in \Omega_k} I\left(\mathrm{y} + \left[\frac{\mathrm{s}}{2}\right] - \mathrm{z}\right)k(\mathrm{z})$$
$$\geq \sum_{\mathrm{z} \in \Omega_k} \min_{\mathrm{y} \in \mathcal{N}(\mathrm{x})} I\left(\mathrm{y} + \left[\frac{\mathrm{s}}{2}\right] - \mathrm{z}\right)k(\mathrm{z})$$
$$\geq \sum_{\mathrm{z} \in \Omega_k} \min_{\mathrm{y} \in \mathcal{N}^\mathcal{I}(\mathrm{x})} I(\mathrm{y})k(\mathrm{z})$$
$$= \sum_{\mathrm{z} \in \Omega_k} D(I)(\mathrm{x})k(\mathrm{z}) = D(I)(\mathrm{x}).$$

$\square$

Property 2. *Let Ω denote the domain of an image I. If there exist some pixels $\mathrm{x} \in \Omega$ such that $I(\mathrm{x}) = 0$, we have*

$$\|D(B)(\mathrm{x})\|_0 > \|D(I)(\mathrm{x})\|_0, \qquad (6)$$

where the L_0 norm $\| \cdot \|_0$ counts the nonzero pixels of $D(I)$.

Proof. In this proof, we exclude the trivial case that the clear image has only zero-intensity pixels.

The derived Property 1 demonstrates that the value of $D(B)(\mathrm{x})$ is larger than that of $D(I)(\mathrm{x})$. As the L_0 norm $\|D(B)(\mathrm{x})\|_0$ counts the number of non-zero elements of $D(B)$, we can directly obtain $\|D(B)(\mathrm{x})\|_0 > \|D(I)(\mathrm{x})\|_0$.

In the following, we discuss the validity of Property 2 when we use the same patch size to compute the dark channels in the clear and blurred images, i.e., $\mathcal{S}_{\mathcal{N}^\mathcal{I}} = \mathcal{S}_{\mathcal{N}}$. Consider a zero-intensity pixel x in the clear image, i.e., $I(\mathrm{x}) = 0$. Let $\mathcal{N}(\mathrm{x})$ denote the patch centered at the pixel x with size the same as the blur kernel. We have $D(I)(\mathrm{x}) = I(\mathrm{x}) = 0$.

Now we show that the corresponding pixel in the blurred image becomes non-zero under mild conditions. We can find a pixel $\mathrm{z}' \in \Omega_k$ that satisfies: $k(\mathrm{z}') \neq 0$ and $I(\mathrm{x} + \left[\frac{\mathrm{s}}{2}\right] - \mathrm{z}') \neq 0$. Thus, we have

$$B(\mathrm{x}) = \sum_{\mathrm{z} \in \Omega_k} I\left(\mathrm{x} + \left[\frac{\mathrm{s}}{2}\right] - \mathrm{z}\right)k(\mathrm{z})$$
$$\geq I\left(\mathrm{x} + \left[\frac{\mathrm{s}}{2}\right] - \mathrm{z}'\right)k(\mathrm{z}') > 0. \qquad (7)$$

$\square$

Remark 1. When the blur kernel is a delta kernel, we always have $B(\mathrm{x}) = I(\mathrm{x})$. Since the goal of this work is to remove blur effect from blurred images, we do not consider this extreme case.

Remark 2. Another explanation for Property 2 is as follows. For a non-delta blur kernel, if $B(\mathrm{x}) = 0$, there should be more than one zero pixels in the neighborhood of x in the clear image I. However, if $I(\mathrm{x}) = 0$, it is not necessarily true that there exists a pixel y in the neighborhood of x in the blurred image B such that $B(\mathrm{y}) = 0$.

We further validate our analysis using a dataset of 3,200 natural images.[1] As shown in Fig. 3, the dark channels of clear images have significantly more zero pixels than those of

---

1. The images are from both the BSDS dataset [33] and the Internet. The datasets are available on the project website, http://vllab1.ucmerced.edu/~jinshan/projects/dark-channel-deblur/.
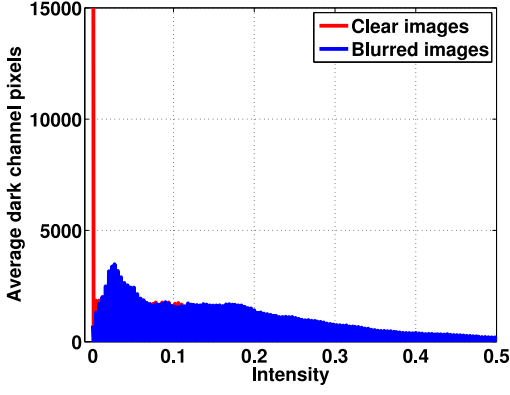
Fig. 3. Intensity histograms for the dark channels of both clear and blurred images in a dataset of 3,200 natural images. Blurred images have significantly fewer zero dark channel pixels than clear ones, which confirms our analysis. The dark channel of each image is computed with an image patch size of 35×35 pixels.
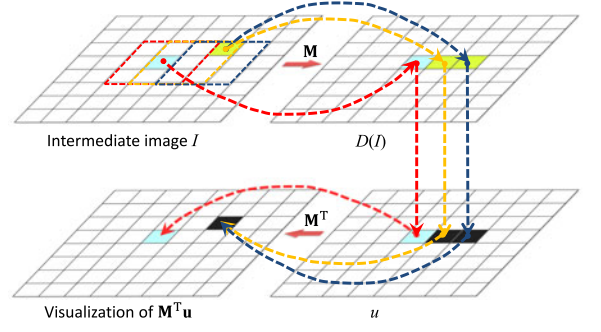

Fig. 4. Top: Computing the dark channel $D(I)$ of an image I by the non-linear $\min$ operator is equivalent to multiplying a binary selection matrix $\mathbf{M}$ with the vectorized image $\mathbf{I}$. The three squares in the intermediate image denote adjacent image patches for computing the dark channel, where the minimum intensity value in each patch is marked with different colors. Bottom: The transpose $\mathbf{M}^\top$ enforces identified dark pixels to be consistent with u.

blurred images. This property also holds for other image types, such as text and saturated images (see Section 7 for the statistics). Thus, the sparsity of dark channels is a natural metric to distinguish clear images from blurred images. This observation motivates us to introduce a new regularization term to enforce sparsity of dark channel in latent images.

4 UNIFORM IMAGE DEBLURRING

Based on the analysis and observations, we use the $\|D(I)\|_0$ norm to measure sparsity of dark channels. We add this constraint to the conventional formulation for image deblurring as

$$\min_{I,k} \|I \otimes k - B\|_2^2 + \gamma\|k\|_2^2 + \mu\|\nabla I\|_0 + \lambda\|D(I)\|_0, \quad (8)$$

where the first term imposes that the convolution output of the recovered image and the blur kernel should be similar to the observation; the second term is used to regularize the solution of the blur kernel; the third term on image gradients retains large gradients and removes tiny details [6], [8]; and γ, μ, as well as λ are weight parameters. We use the coordinate descent method to alternatively compute the latent image I

$$\min_{I} \|I \otimes k - B\|_2^2 + \mu\|\nabla I\|_0 + \lambda\|D(I)\|_0, \quad (9)$$

and the blur kernel k

$$\min_{k} \|I \otimes k - B\|_2^2 + \gamma\|k\|_2^2. \quad (10)$$

4.1 Estimating the Latent Image I

Minimizing (9) is computationally intractable due to the L_0-regularized term and the non-linear function $D(\cdot)$. To solve optimization problem with the L_0-regularized term, we use the half-quadratic splitting L_0 minimization approach [34]. Similar to [6], [35], we introduce the auxiliary variables u with respect to $D(I)$ and $g = (g_h, g_v)$ corresponding to image gradients in the horizontal and vertical directions. The objective function (9) can be rewritten as

$$\min_{I,u,g} \|I \otimes k - B\|_2^2 + \alpha\|\nabla I - g\|_2^2$$
$$+ \beta\|D(I) - u\|_2^2 + \mu\|g\|_0 + \lambda\|u\|_0, \quad (11)$$

where α and β are penalty parameters. When α and β are close to infinity, the solution of (11) approaches to that of (9) [36]. We can solve (11) by alternatively minimizing I, u, and g while fixing the other variables. Note that given I, the subproblems of solving for the auxiliary variables u and g do not involve the nonlinear function $D(\cdot)$.

We solve I with the nonlinear $\min$ operator as follows:

$$\min_{I} \|I \otimes k - B\|_2^2 + \alpha\|\nabla I - g\|_2^2 + \beta\|D(I) - u\|_2^2. \quad (12)$$

Our observation is that the non-linear operation $D(I)$ is equivalent to a linear operator $\mathbf{M}$ applied to the vectorized image $\mathbf{I}$. For consistency, we use $\mathbf{D}(\mathbf{I})$ to denote the vector form of $D(I)$. Let $y = \operatorname{argmin}_{z \in \mathcal{N}(x)} I(z)$. $\mathbf{M}$ satisfies

$$\mathbf{M}(\mathrm{x}, \mathrm{z}) = \begin{cases} 1, & \mathrm{z} = \mathrm{y}, \\ 0, & otherwise. \end{cases} \quad (13)$$

Multiplying the xth row of $\mathbf{M}$ with $\mathbf{I}$ gives the value of the pixel y, i.e., $\mathbf{I}(y)$ or equivalently $\mathbf{D}(\mathbf{I})(x)$ (see the top row of Fig. 4). Given the previous estimated intermediate latent image, we can construct the desired matrix $\mathbf{M}$ according to (13), as shown in Fig. 4.

For the clear image, $\mathbf{MI} = \mathbf{D}(\mathbf{I})$ strictly holds. Without the clear image, we compute an approximation of $\mathbf{M}$ using the intermediate result at each iteration. As the intermediate result becomes closer to the clear image, $\mathbf{M}$ approaches to the desired D. Empirically, we find that the approximation scheme converges well, as shown in Fig. 16.

Given the selection matrix $\mathbf{M}$, we solve I by

$$\min_{\mathbf{I}} \|\mathbf{T}_k\mathbf{I} - \mathbf{B}\|_2^2 + \alpha\|\nabla\mathbf{I} - \mathbf{g}\|_2^2 + \beta\|\mathbf{MI} - \mathbf{u}\|_2^2, \quad (14)$$

where $\mathbf{T}_k$ is a Toeplitz (convolution) matrix of k, $\mathbf{B}$, $\mathbf{g}$, and $\mathbf{u}$ denote vector forms of B, g, and u, respectively. The matrix-vector product with respect to the Toeplitz matrix can be computed using the Fast Fourier Transform (FFT) [36]. The solution of (14) can be obtained according to [6], [7], [8].

Given I, we compute u and g separately by

$$\min_{u} \beta\|D(I) - u\|_2^2 + \lambda\|u\|_0,$$
$$\min_{g} \alpha\|\nabla I - g\|_2^2 + \mu\|g\|_0. \quad (15)$$

We note that (15) is an element-wise minimization problem. Thus, the solution of u is

$$u = \begin{cases} D(I), & |D(I)|^2 \geqslant \frac{\lambda}{\beta}, \\ 0, & \text{otherwise}, \end{cases} \quad (16)$$

and similarly for the solution of g is

$$g = \begin{cases} D(I), & \|\nabla I\|^2 \geqslant \frac{\mu}{\alpha}, \\ 0, & \text{otherwise}. \end{cases} \quad (17)$$

Algorithm 1 summarizes the main steps for solving (11). In Algorithm 1, we pose the sub-problem g in the inner loop as this scheme enforces smooth results with fewer artifacts in the recovered image [37].

Algorithm 1. Algorithm for Solving (11)

Input: Blurred image B and blur kernel k.
$I \leftarrow B, \beta \leftarrow \beta_0$.
repeat
  solve $D(I)$ according to the definition of dark channel
  and build matrix $\mathbf{M}$ according to (13).
  solve u using (16).
  $\alpha \leftarrow \alpha_0$.
  repeat
    solve g using (17).
    solve I using (14).
    $\alpha \leftarrow 2\alpha$.
  until $\alpha > \alpha_{\max}$
  $\beta \leftarrow 2\beta$.
until $\beta > \beta_{\max}$
Output: Intermediate latent image I.

4.2 Estimating Blur Kernel k

Given I, the kernel estimation in (10) is a least squares minimization problem. We note that kernel estimation methods based on gradients have been shown to be more accurate [5], [8], [10] (see analysis in Section 7). Thus, we estimate the blur kernel k by

$$\min_k \|\nabla I \otimes k - \nabla B\|_2^2 + \gamma \|k\|_2^2. \quad (18)$$

Similar to existing approaches [6], [8], [10], we obtain the solution of (18) by FFTs. After obtaining k, we set the negative elements of k to 0, and normalize k so that k satisfies our definition of the blur kernel. Similar to the state-of-the-art methods, the proposed kernel estimation process is carried out in a coarse-to-fine manner using an image pyramid [10]. Algorithm 2 shows the main steps for the kernel estimation algorithm on one pyramid level.

Algorithm 2. Blur Kernel Estimation Algorithm

Input: Blurred image B.
initialize k with results from the coarser level.
while $i \leq \text{max\_iter}$ **do**
  solve I using (11).
  solve k using (18).
end while
Output: Blur kernel k.

---

5 NON-UNIFORM IMAGE DEBLURRING

The proposed method can be easily extended to handle non-uniform deblurring where the blurred images are acquired from moving cameras (e.g., rotational and translational movements) [38], [39], [40], [41], [42]. Based on the geometric model of camera motion [41], [42], the non-uniform blur model can be expressed as

$$\mathbf{B} = \sum_t k_t \mathbf{H}_t \mathbf{I} + \mathbf{n}, \quad (19)$$

where $\mathbf{I}$ and $\mathbf{n}$ denote vector forms of I, n in (1); t is the index of camera pose samples; $\mathbf{H}_t$ is a matrix derived from the homography matrix in [42]; and k_t is the weight corresponding to the tth camera pose which satisfies $k_t \geq 0$ and $\sum_t k_t = 1$. Similar to [42], (19) can be expressed as

$$\mathbf{B} = \mathbf{KI} + \mathbf{n} = \mathbf{Ak} + \mathbf{n}, \quad (20)$$

where $\mathbf{k}$ is a vector and its element is composed of the weight k_t. Based on (20), the non-uniform deblurring process is achieved by alternatively minimizing

$$\min_{\mathbf{I}} \|\mathbf{KI} - \mathbf{B}\|_2^2 + \lambda \|\mathbf{D}(\mathbf{I})\|_0 + \mu \|\nabla \mathbf{I}\|_0, \quad (21)$$

and

$$\min_{\mathbf{k}} \|\mathbf{Ak} - \mathbf{B}\|_2^2 + \gamma \|\mathbf{k}\|_2^2. \quad (22)$$

We use the fast forward approximation method [39] to estimate the latent image $\mathbf{I}$ and the weight $\mathbf{k}$. The algorithmic details are presented in the supplementary material, which can be found on the Computer Society Digital Library at http://doi.ieeecomputersociety.org/10.1109/TPAMI.2017.2753804.

6 EXPERIMENTAL RESULTS

We evaluate the proposed algorithm against state-of-the-art natural image deblurring methods on two natural image deblurring datasets [17], [18]. In addition, we evaluate the proposed method using text [6], face [13], and low-illumination [16] images and compare it to approaches designed specifically for these tasks. Finally, we present results on images with non-uniform blurs. The MATLAB code is available on the project web site http://vllab1.ucmerced.edu/~jinshan/projects/dark-channel-deblur/and more results can be found in the supplementary document, available online.

Parameter Setting. In all experiments, we set $\lambda = \mu = 0.004$, $\gamma = 2$, and the neighborhood size to compute the dark channel in (2) to be 35 (see Section 7 for analysis). We empirically set $\text{max\_iter} = 5$ as a trade-off between accuracy and speed. We use the same settings as [37] for the parameters: α_0, β_0, $\alpha_{\max}$, and $\beta_{\max}$. Similar to [3], [9], [11], we use a non-blind deblurring method to recover the final latent images with the kernels estimated by the proposed algorithm. In all experiments, we use the non-blind deblurring algorithm [6] unless mentioned otherwise.

Natural Images. We use the image dataset by Köhler et al. [17] which contains 4 images and 12 blur kernels. The PSNR value is computed by comparing each restored image with 199 clear images captured along the camera
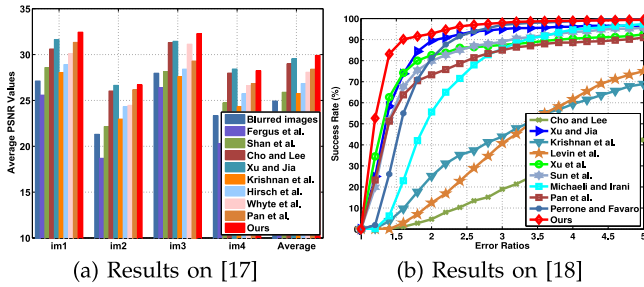
(a) Results on [17]   (b) Results on [18]

Fig. 5. Quantitative evaluations on two benchmark datasets. Our method performs competitively against the state-of-the-art methods.

motion trajectory. As shown in Fig. 5a, the proposed algorithm performs well in terms of PSNR. Fig. 6 shows results on a challenging example with significant blur. Although the state-of-the-art methods [10], [11] are able to deal with large blur in most regions, their deblurred images contain moderate ringing artifacts. In contrast, the image deblurred by the proposed algorithm contains fewer artifacts and clearer details.

We next evaluate the proposed algorithm on the dataset by Sun et al. [18] which contains 80 images and 8 blur kernels. For fair comparisons, we use the provided code of the state-of-the-art methods [4], [5], [6], [8], [10], [11], [12], [18] to estimate blur kernels and the non-blind deblurring algorithm [43] to generate the final deblurring results. We use the error ratio [9] for performance evaluation. As Fig. 5b shows, the proposed algorithm performs favorably against the state-of-the-art methods. We show the error ratio values of the best three algorithms in Table 1. Among 640 blurred

images, our algorithm fails on one image in which the error ratio value is larger than 6.2.

We evaluate the proposed algorithm using a real natural image (Fig. 7). We use the same non-blind deconvolution method [6] with blur kernels estimated by each evaluated algorithm. While the deblurred results by the state-of-the-art methods [4], [6], [8] contain strong ringing artifacts and blur effects, the image generated by the proposed algorithm is clearer. The deblurred image by our method without the dark channel prior contains considerable artifacts, which shows the effectiveness of the dark channel prior.

Text Images. Table 2 shows the PSNR results of the evaluated methods on the text image dataset [6], which contains 15 clear images and 8 blur kernels. The PSNR by the proposed algorithm is higher than those by other natural image deblurring methods [4], [5], [10], [11] and 0.9 dB lower than that by the scheme designed specifically for text images [6]. Fig. 8 shows the results by the proposed algorithm and the state-of-the-art methods for natural and text images.

Low-Illumination Images. Blurred images captured in low-illumination scenes are particularly challenging as saturated pixels often exist and edges cannot be easily extracted by most deblurring methods for kernel estimation [16], [47]. For example, the kernel estimated by [8] is similar to a delta kernel due to the effect of saturated regions as shown in Fig. 9b and the deblurred image contains significant residual blur. Compared with the clean image, the dark channel of the blurred one with saturated regions is also less sparse. As a result, the deblurred images by the proposed algorithm

(a) Input   (b) Cho and Lee [10]   (c) Xu and Jia [11]   (d) Ours without $D(I)$ (e) Ours with $D(I)$
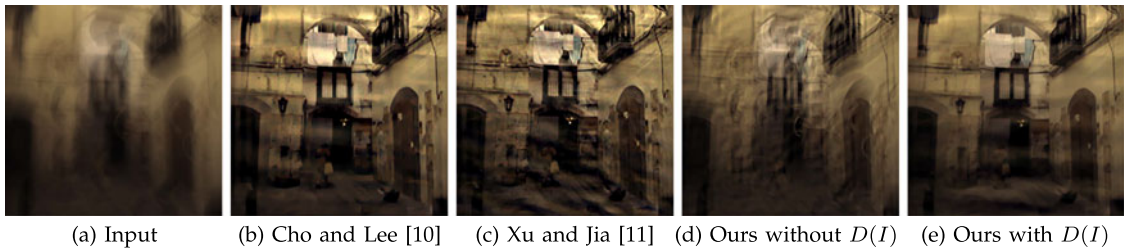
Fig. 6. Deblurred results using one challenging image from the dataset [17]. The deblurred images by other methods are obtained from the reported results in [17]. The recovered image by the proposed algorithm with the dark channel prior is clearer.

TABLE 1
Success Rates of the Best Three Algorithms on the Dataset [18]

Error ratio	≤ 1.5	≤ 2	≤ 2.5	≤ 3	≤ 3.5	≤ 4	≤ 4.5	≤ 5	≤ 6.2
Sun et al. [18]	388/640	511/640	550/640	569/640	587/640	599/640	607/640	612/640	624/640
Perrone and Favaro [44]	261/640	520/640	594/640	621/640	628/640	632/640	637/640	637/640	639/640
Ours	568/640	594/640	621/640	627/640	632/640	633/640	635/640	636/640	639/640

(a) Input   (b) Krishnan et al. [4]   (c) Xu et al. [8]   (d) Pan et al. [6]   (e) Ours without $D(I)$ (f) Ours with $D(I)$
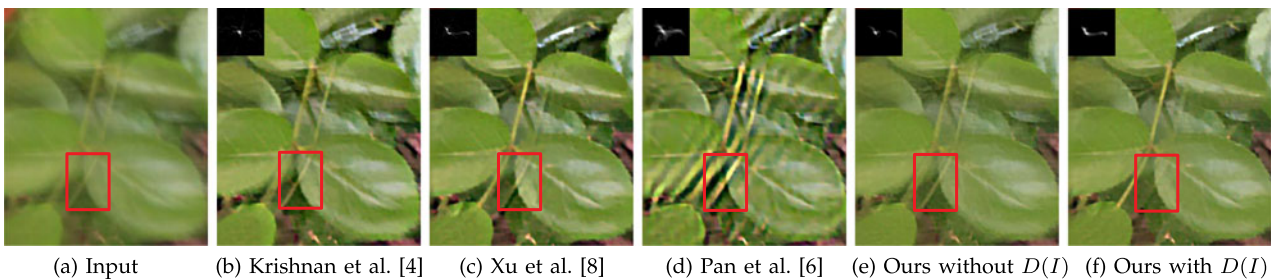
Fig. 7. Deblurred results on a real natural image. The parts in red boxes (b)-(e) contain significant residual blur.

TABLE 2
Quantitative Evaluations on the Text Image Dataset [6]

	Cho and Lee [10]	Xu and Jia [11]	Krishnan et al. [4]	Levin et al. [5]	Xiao et al. [45]	Pan et al. [6]	Ours
PSNR (dB)	23.80	26.21	20.86	24.90	27.56	28.80	27.94

The proposed algorithm performs favorably against recent deblurring methods for natural images and the method designed for text images [6].
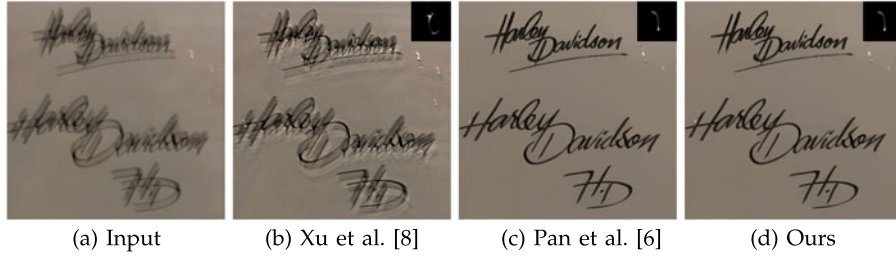

(a) Input (b) Xu et al. [8] (c) Pan et al. [6] (d) Ours

Fig. 8. On real text images, the proposed generic algorithm generates results comparable to methods designed specifically for this scenario.

(a) Input (b) Xu et al. [8] (c) Hu et al. [16] (d) Ours
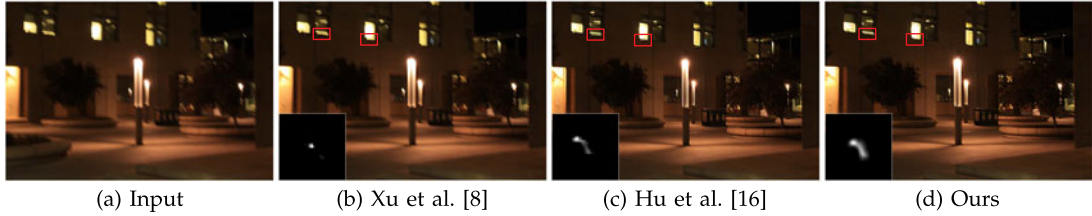
Fig. 9. Results on a real saturated image. The deblurring results are all generated by the non-blind deconvolution method [16]. Residual blur and ringing artifacts exist in the red boxes in (b)-(c).

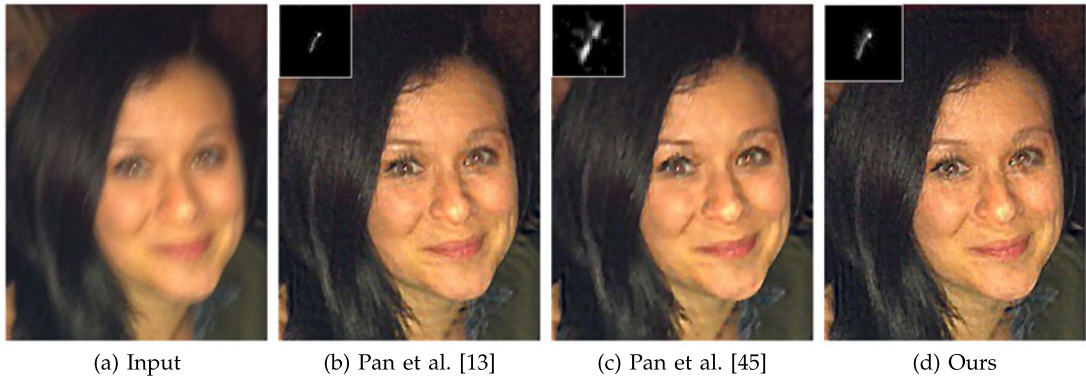(a) Input (b) Pan et al. [13] (c) Pan et al. [45] (d) Ours

Fig. 10. Deblurring real face images. The proposed algorithm performs favorably against a method that uses a face dataset to explore face structures for deblurring [13].

are comparable to [16] which is designed specifically for low-light conditions.

Face Images. We evaluate the proposed algorithm on face images against methods designed for this particular class. As shown in Fig. 10, the proposed generic algorithm performs well against the method which explicitly exploits facial structures using an exemplar dataset [13].

Non-Uniform Deblurring. As our method can be easily extended to deal with non-uniform blur, we present results on an image degraded by spatially-variant motion blur in Fig. 11 (see the supplemental material for more examples and large images, available online). Compared with the state-of-the-art non-uniform deblurring method [8], the proposed algorithm generates images with fewer artifacts and clearer textures.

7 ANALYSIS AND DISCUSSIONS

In this section, we analyze the proposed algorithm based on the dark channel prior with comparisons to the state-of-the-art methods. We explain why the proposed prior is effective for image deblurring and discuss the limitations.

Effectiveness of the Dark Channel Prior. Our method without the dark channel prior can be considered as the deblurring scheme by Xu et al. [8]. We remove the dark channel prior in the proposed method for comparisons. As shown in Figs. 12f and 12g, the use of the dark channel prior helps generate intermediate results with sharper edges and facilitates kernel estimation. In addition, the dark channel of the intermediate results becomes more sparse with more iterations (Fig. 12h).
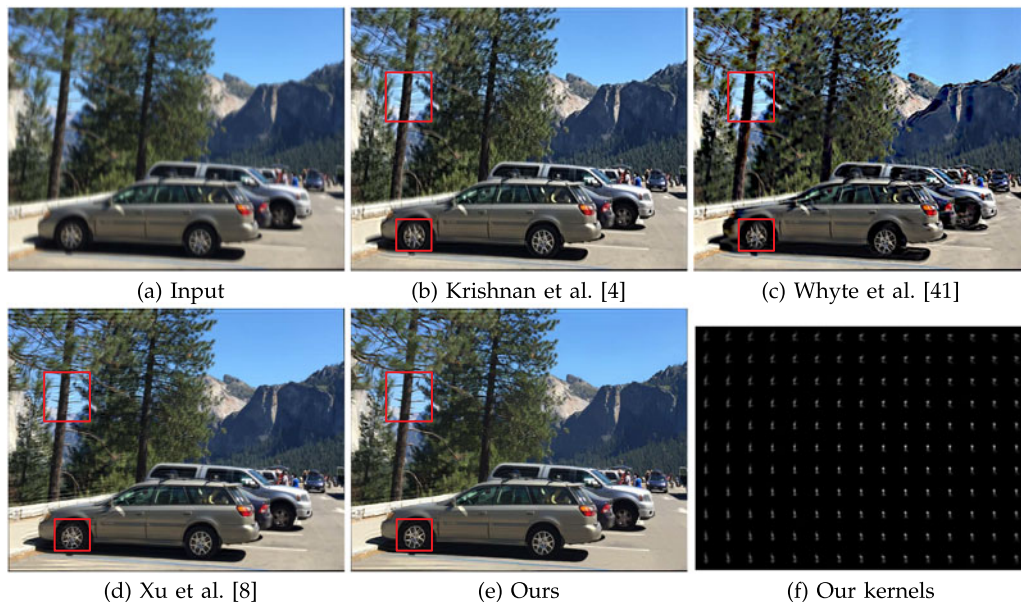
Fig. 11. Proposed dark channel prior for images with non-uniform blur. The regions enclosed in red boxes of (b)-(d) contain ringing artifacts and residual blurs (best viewed on high-resolution display with zoom-in).

We quantitatively evaluate the proposed method with and without the dark channel prior using two benchmark datasets [9], [17]. Fig. 13 shows that the dark channel prior consistently helps improve image deblurring. In particular, the proposed method with the dark channel prior achieves 100 percent success rate on the dataset by Levin et al. [9] at an error ratio of 2. All these results demonstrate the effectiveness of the proposed deblurring algorithm based on the dark channel prior.

Favored Minimum of the Energy Function. The dark channel prior is effective for deblurring because it helps compute lower energy for clear images than for blurred ones. Two methods [4], [12] also have energy functions with similar properties. However, these are mainly designed for natural images and less effective for specific scenarios (e.g., text and low-illumination images). For example, the energy computed by the normalized sparsity prior [4] for clear natural images is lower than that for blurred images, but not always so for clear text images (Fig. 14b). In contrast, the text images (Fig. 14a) are favored by the dark channel prior due to lower energy. In [12], internal patch recurrence is exploited for image deblurring. This method performs well when images contain repetitive patterns among patches, but may fail otherwise. Our analysis and observation show that the dark channel prior can be broadly applied to scenarios where blur makes the dark channel less sparse.

He et al. apply the dark channel prior to image dehazing [32]. The assumption that all the pixel values of the dark channel are zero mainly holds for outdoor haze-free images. In contrast, our analysis shows that the blur operation makes the dark channel of clean images less sparse. Thus, we assume that the dark channel of clear images is sparse. Empirically, this assumption holds not only for natural images, but also for specific scenarios including text and saturated images (Fig. 14a). We note that the dark channel prior and domain specific knowledge are more likely to be complementary than contradictory, which will be exploited in our future work.

Relation with L_0-Regularized Deblurring Methods. Two methods [6], [8] use L_0-regularized priors for deblurring. The method [8] assumes L_0 sparsity on image gradients, which performs well on natural images but less effectively on text images (Fig. 8b). On the other hand, the method [6] assumes L_0 sparsity on both the intensity and gradients for deblurring text images. The L_0-regularized intensity term plays a key role in text image deblurring as the intensity values (histograms) of text images are close to two-tone. However, the intensity histograms of natural images are more complex than those of text images, and this prior is not applicable to natural image deblurring problems (Fig. 7d). The intermediate results in Fig. 12e show that although this L_0-regularized intensity term helps preserve significant contrast compared to (f), it fails to recover useful structures for kernel estimation.

Sparsity Constraints on the Dark Channel Prior. According to Property 2 in Section 3, the pixel values of the dark channel of clear images become denser by the convolution operator. We note that the L_1 norm is usually used to model sparsity. Thus, we apply the L_1 norm on the dark channel (i.e., $\|D(I)\|_1$) to illustrate its effect on kernel estimation. To demonstrate the effect of $\|D(I)\|_0$ and $\|D(I)\|_1$, we quantitatively evaluate our method with these two constraints using the dataset by Levin et al. [9]. As shown in Fig. 15a, the method with $\|D(I)\|_0$ or $\|D(I)\|_1$ achieves better results than the method without using the dark channel prior, which demonstrates that the sparsity of dark channel is an inherent property and able to help blur kernel estimation. Note that the method using $\|D(I)\|_0$ performs best as $\|D(I)\|_0$ tends to lead to more sparse solutions than those of $\|D(I)\|_1$.

In addition, we apply the L_1 norm to both dark channel values and image gradients. Fig. 15b demonstrates the method when using L_1 norm on both dark channel and image gradients is less effective as the L_1 norm on image gradients usually favors trivial solutions within the MAP framework [9].

(a) Input   (b) Xu et al. [8]   (c) Pan et al. [6]   (d) Ours

(e) Intermediate results of [6]

(f) Intermediate deblurred results by our method without using the dark channel prior

(g) Intermediate deblurred results by our method using the dark channel prior

(h) Dark channels of the intermediate deblurred images

Fig. 12. Deblurred images by the evaluated methods are shown in (a)-(d), and the intermediate results over iterations (from left to right) are shown in (e)-(h). With the dark channel prior, our method recovers intermediate results containing sharper edges for kernel estimation. The dark channels of the intermediate results become darker, which favor clear images and facilitate kernel estimation.

We evaluate the effect of image gradient and blur regularization (i.e., $\|k\|_2^2$) in the proposed model. Fig. 15b shows that the proposed algorithm performs slightly better than the proposed method without using $\|k\|_2^2$. The proposed method does not perform well when both the blur and the gradient prior terms are removed. This is because the dark channel only captures pixel statistics in an image patch. It cannot model the structures of an image well (e.g., edges), which is better captured by the image gradient prior.

Convergence Property. As our energy function is nonlinear and non-convex, a natural question is whether the proposed optimization method converges well or not. We quantitatively evaluate convergence properties of our method on the benchmark dataset by Levin et al. [9].

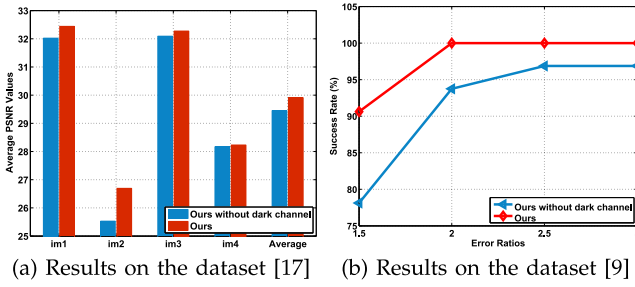(a) Results on the dataset [17]   (b) Results on the dataset [9]

Fig. 13. Quantitative results of our method with and without the dark channel prior on two benchmark datasets. The dark channel prior consistently helps improve the results. In particular, our method with the dark channel prior has 100 percent success at error ratio 2 on the dataset by Levin et al. [9].
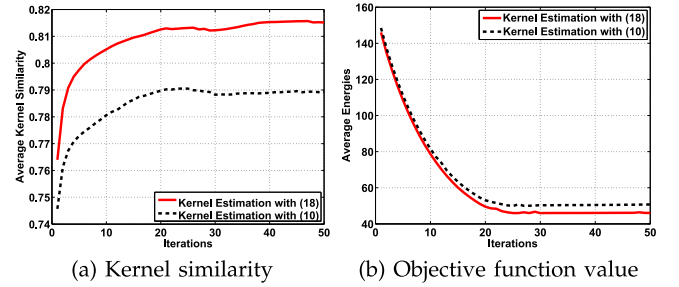

(a) Dark channel on datasets [6] and [16]

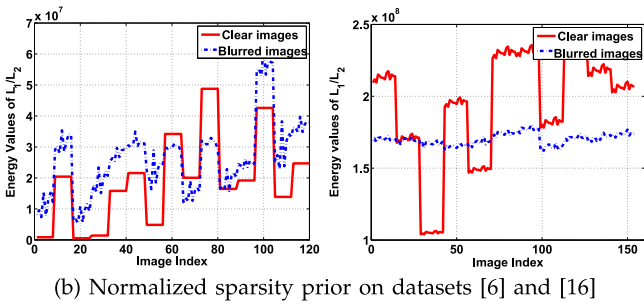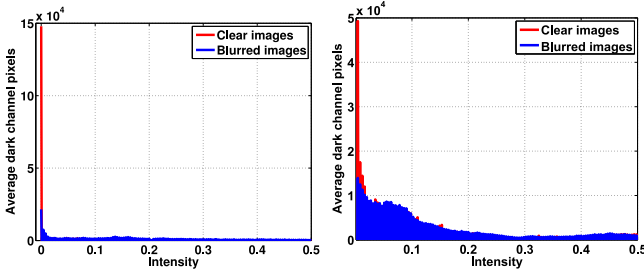(b) Normalized sparsity prior on datasets [6] and [16]

Fig. 14. Statistics of the dark channel and normalized sparsity [4] priors on text (top) and low-illumination (bottom) images. The statistics confirm our analysis that the proposed dark channel prior favors clear images over blurred ones. However, this property does not hold for the normalized sparsity prior [4] (i.e., L_1/L_2) on text and low-illumination images and sometimes favors blurred images.

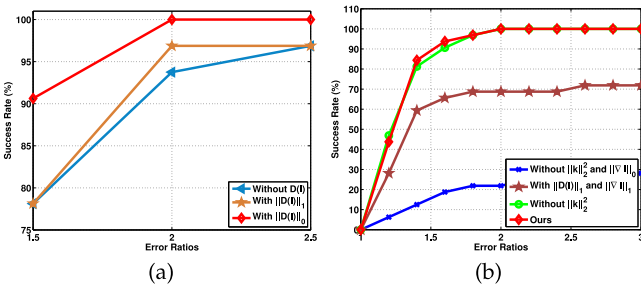(a)   (b)

Fig. 15. Quantitative evaluation on sparsity constraints of the dark channel prior and image gradient using the benchmark dataset [9]. (a) Results generated by different sparsity constraints on the dark channel. (b) Results generated by different sparsity constraints on image gradients and without or without $\|k\|_2^2$. The methods with $\|D(I)\|_0$ leads to more sparse solutions and better results.

Figs. 16a and 16b show that the proposed method converges after 50 iterations, in terms of average kernel similarity values [48] and energy computed from (8). However, the kernel estimates generated by image gradients have

(a) Kernel similarity   (b) Objective function value

Fig. 16. Fast convergence of our method, which empirically validates the approximated non-linear operator in this work. The kernel estimation step by image gradients (i.e., (18)) is able to generate the results with higher kernel similarity values and lower energy values, which indicates the importance of image gradients for kernel estimation.

TABLE 3
Run-Time (in second) Performance

Method	255×255	600×600	800×800
Xu et al. [8]	2.11	6.96	21.36
Krishnan et al. [4]	24.23	111.09	226.58
Levin et al. [9]	117.06	481.48	917.84
Ours without $D(I)$	2.77	15.65	28.94
Ours-naive	134.31	691.71	964.90
Ours	17.07	115.86	195.80

All the algorithms are implemented in MATLAB.

TABLE 4
Evaluation of Patch Size on the Dataset [9]

Patch size	15×15	25×25	35×35	45×45
Avg. PSNR	30.79	30.95	31.08	30.92

higher kernel similarity values and lower energy, which suggest multiple local minima exist. In this work, we use image gradients (i.e., (18)) to estimate blur kernels as it performs better. Our future work will analyze the local minima of the energy function and develop better optimization schemes.

Computational Complexity. Compared to the L_0-regularized methods [6], [8], the proposed algorithm requires computing the dark channel and look-up table. The complexity of this step is $O(N)$ and independent of patch size [49] where N is the number of pixels. This is the main computational bottleneck, and other steps can be accelerated by FFTs. The proposed method requires 17 seconds to deblur a 255×255 image on a machine with an Intel Core i7-4790 processor and 28 GB RAM. Table 3 shows that the run-time of the evaluated methods. Note that the time to compute $D(I)$ and $\mathbf{M}$ based on [49] is less than that with the naive implementations of $D(I)$ and $\mathbf{M}$.

Effect of Patch Size for Computing $D(I)$. We analyze the effect of patch size as it is one of the important factors for computing the dark channel. We carry out experiments on the dataset [9] with different patch size. Table 4 shows the quantitative results of the deblurred images based on PSNR. Note that the image resolution in [9] is 255×255 pixels and we only evaluate a maximum patch size of 45 pixels in this dataset. Overall, the proposed algorithm is insensitive to patch size variation within a reasonable range.
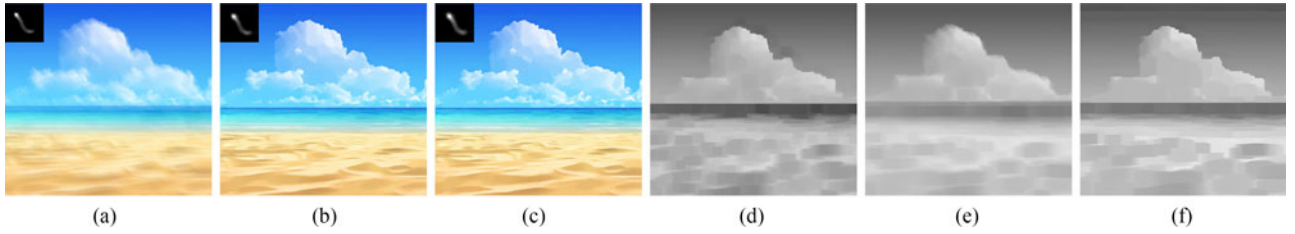
Fig. 17. One limitation of the proposed method on a synthetic image. (a) Blurred image and blur kernel. (b) Ours without using the dark channel prior. (c) Ours using the dark channel prior. (d) Dark channel of clear image. (e) Dark channel of blurred image. (f) Our estimated dark channel. As the dark channel of this clear image does not contain zero-elements in this synthetic image, the derivation of Property 2 does not hold. For such cases, we always have $\|D(B)\|_0 = \|D(I)\|_0$. The dark channel prior does not help kernel estimation and deblurring results generated with and without dark channel prior are similar.

(a) Blurred image   (b) Ours without using $D(I)$ (c) Ours using $D(I)$ (d) Ours with Gaussian filter
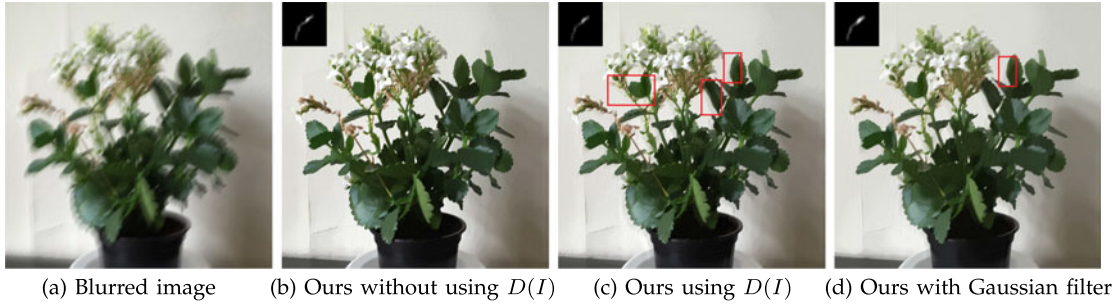
Fig. 18. The proposed dark channel prior is sensitive to Gaussian noise. Since the noise will change the minimum intensity value of an image patch, the deblurred image generated with the dark channel prior is still blurry as shown in the parts in red boxes in (c), while the deblurred image generated without using the dark channel prior is much clearer. We note that although the estimated kernel contains less noise after applying Gaussian filter on the blurred input, the final deblurred image is over-smoothed and contains ringing artifacts as shown in the red box in (d) due to the filter effect.
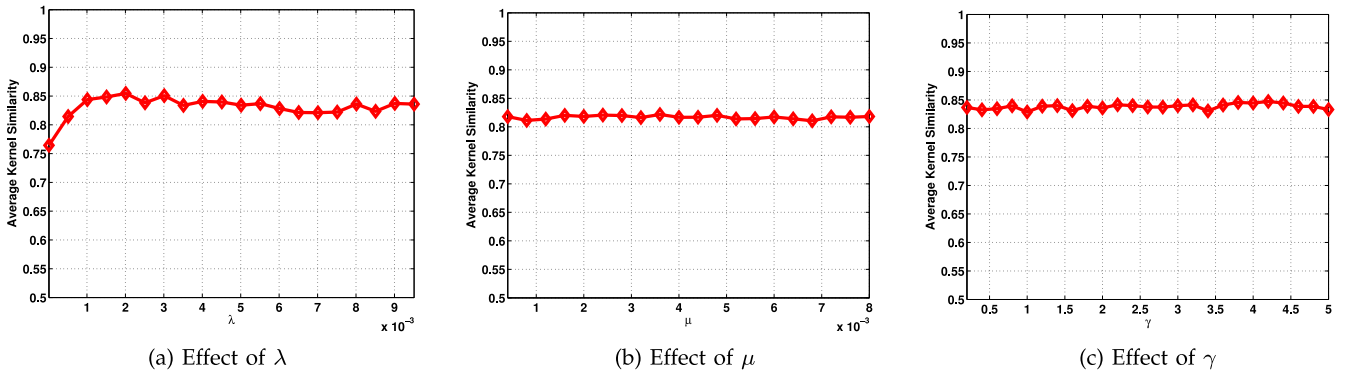

(a) Effect of λ (b) Effect of μ (c) Effect of γ

Fig. 19. Sensitivity analysis with respect to parameters γ, μ, and λ in the proposed algorithm.

Parameter Analysis. The proposed model involves three main parameters, γ, μ, and λ. We evaluate the effects of these parameters on image deblurring using the dataset [9] by varying one and fixing the others with the kernel similarity metric to measure the accuracy of estimated kernels. Fig. 19 shows the proposed deblurring algorithm based on the dark channel prior is insensitive to parameter settings.

Limitations. Despite the robust performance on a variety of challenging datasets, the proposed algorithm does not perform well when a clear image has no dark pixels. In such cases, the dark channel prior is less likely to help kernel estimation as Property 2 does not hold, i.e., $\|D(B)(x)\|_0 = \|D(I)(x)\|_0$. The solution of u given by (16) is likely to be $D(I)$ as the value of $\frac{\lambda}{\beta}$ will be much smaller than that of $D(I)$. Thus, the constraint $\|D(I)\|_0$ would have no effect on the intermediate latent image estimation. As a result, the deblurred images by our method with and without the dark channel are similar. Fig. 17 shows a synthetic example where the latent image does not contain dark pixels. The deblurred results with and without dark channel prior are almost the same.

The proposed method fails gracefully when the dark channel of the original image is not sparse.

In addition, the proposed method assumes that only the blur process changes the sparsity of the dark channel. Significant noise may affect the dark pixels of an image, which accordingly affects kernel estimation. Fig. 18 shows an example which contains Gaussian noise. Our method without using the dark channel prior generates a much clearer deblurred image. In contrast, the deblurred image generated using the dark channel prior still contains blur, which indicates that the proposed method based on the dark channel prior is not robust to image noise.

We evaluate the proposed method on blurred images with different Gaussian noise levels. We use the dataset by Levin et al. [9] and add Gaussian noise for each image, where the noise level ranges from 0 to 10 percent. Fig. 20 shows that the proposed algorithm performs well when the noise level is low but degrades when the noise level is high. Our future work will consider joint deblurring and denoising using the dark channel prior.
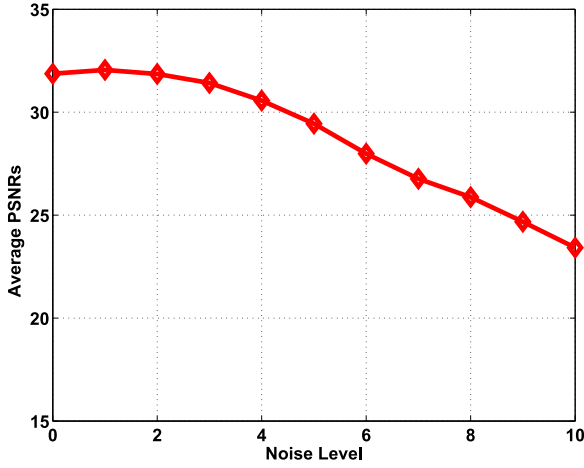
Fig. 20. Evaluations on the noisy blurred images.

(a) Input   (b) He et al. [32]
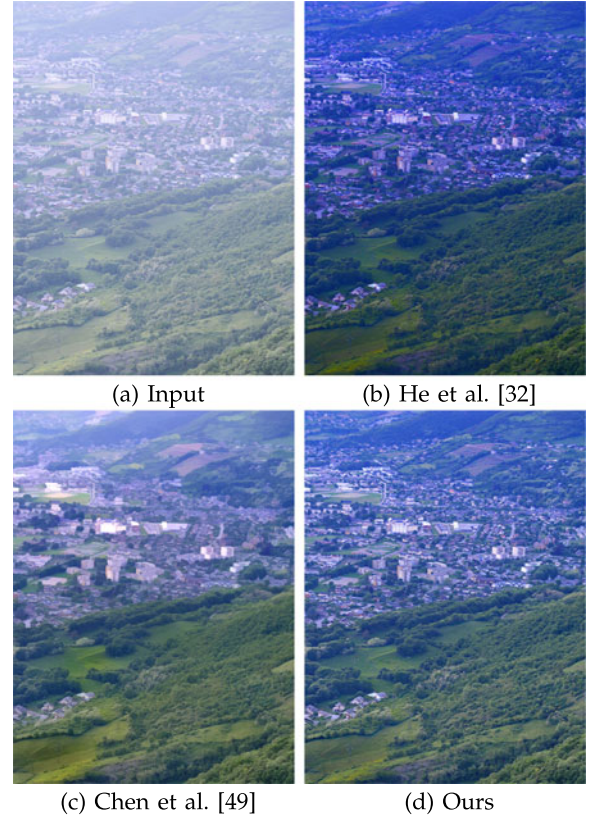
(c) Chen et al. [49]   (d) Ours

Fig. 21. Proposed dark channel prior for image dehazing. The dehazed images by the proposed algorithm are clearer and contains more details compared to the result in (c).

8 IMAGE DEHAZING

According to the analysis in Section 3, the dark channel of clear images has the sparsity property. Thus, it can be naturally applied to image dehazing as the dark channel of hazy images are not sparse [32]. We use the conventional formulation for hazy images

$$J(\mathbf{x}) = I(\mathbf{x})t(\mathbf{x}) + A(1 - t(\mathbf{x})), \qquad (23)$$

where $J(\mathbf{x})$, $I(\mathbf{x})$, $t(\mathbf{x})$, and A denote the hazy image, clear image, transmission map, and atmospheric light, respectively.

We note $t(\mathbf{x})$ in [32] is computed based on the assumption that all the dark channel values of I are zero. For pixels with non-zero dark channel in the clear images, the transmission map $t(\mathbf{x})$ is under-estimated according to (12) in [32]. Using (23), the dehazed image is directly computed by $I(\mathbf{x}) = \frac{J(\mathbf{x}) - A}{t(\mathbf{x})} + A$. The inequality $J(\mathbf{x}) - A \leq 0$ holds for most pixels as the values of A are usually estimated using the brightest pixel of $J(\mathbf{x})$. When $t(\mathbf{x})$ is under-estimated, the estimated $I(\mathbf{x})$ would be smaller than the ground truth and thus the dehazed images look darker.

Instead of directly restoring I from (23), we use the model

$$\min_{I(\mathbf{x})} \|J(\mathbf{x}) - I(\mathbf{x})t(\mathbf{x}) - A(1 - t(\mathbf{x}))\|_2^2 + \theta\|D(I)\|_0, \qquad (24)$$

to reconstruct $I(\mathbf{x})$. The transmission map and atmospheric light are computed based on [32]. We use the half-quadratic splitting method to solve (24) and set θ to be 0.01 in the experiments. Restoring I from (24) means that we do not require all the dark channel values of I to be zero. Thus the dehazed images are brighter (closer to the original) than those by [32].

We evaluate the proposed method against the approach based on the dark channel prior [32] using real hazy images (Fig. 21). Instead of directly reconstructing clear images using the hazy model [32], the proposed algorithm restores brighter clear images by solving (24) (Fig. 21d). In addition, the proposed algorithm performs favorably against a recent method [50]. More results can be found in the supplementary material, available online.

9 CONCLUDING REMARKS

Motivated by an analysis of the convolution operation and the effect on the dark channel of blurred images, we introduce an effective blind image deblurring algorithm. The proposed dark channel prior models the changes to blurred images caused by the blur process and favors clear images over blurred ones in the deblurring process. To restore images regularized by the dark channel prior, we develop an effective optimization algorithm based on a half-quadratic splitting method and look-up tables. The proposed algorithm does not require heuristic edge selection steps or complex processing techniques in kernel estimation. Furthermore, the proposed algorithm can be easily extended to non-uniform image deblurring. The proposed algorithm performs favorably against the state-of-the-art methods developed for natural images and specific scenarios. In addition, we show that the proposed dark channel prior can be applied to image dehazing to generate sharper and brighter results.

REFERENCES

[1] L. B. Lucy, "An iterative technique for the rectification of observed distributions," *Astronomy J.*, vol. 79, no. 6, pp. 745–754, 1974.

[2] T. Chan and C. Wong, "Total variation blind deconvolution," *IEEE Trans. Image Process.*, vol. 7, no. 3, pp. 370–375, Mar. 1998.

[3] R. Fergus, B. Singh, A. Hertzmann, S. T. Roweis, and W. T. Freeman, "Removing camera shake from a single photograph," *ACM SIGGRAPH*, vol. 25, no. 3, pp. 787–794, 2006.

[4] D. Krishnan, T. Tay, and R. Fergus, "Blind deconvolution using a normalized sparsity measure," in *Proc. IEEE Conf. Comput. Vis. Pattern Recognit.*, 2011, pp. 2657–2664.

[5] A. Levin, Y. Weiss, F. Durand, and W. T. Freeman, "Efficient marginal likelihood optimization in blind deconvolution," in *Proc. IEEE Conf. Comput. Vis. Pattern Recognit.*, 2011, pp. 2657–2664.

[6] J. Pan, Z. Hu, Z. Su, and M.-H. Yang, "Deblurring text images via L_0-regularized intensity and gradient prior," in *Proc. IEEE Conf. Comput. Vis. Pattern Recognit.*, 2014, pp. 2901–2908.

[7] Q. Shan, J. Jia, and A. Agarwala, "High-quality motion deblurring from a single image," *ACM SIGGRAPH*, vol. 27, no. 3, 2008, Art. no. 73.

[8] L. Xu, S. Zheng, and J. Jia, "Unnatural L_0 sparse representation for natural image deblurring," in *Proc. IEEE Conf. Comput. Vis. Pattern Recognit.*, 2013, pp. 1107–1114.

[9] A. Levin, Y. Weiss, F. Durand, and W. T. Freeman, "Understanding and evaluating blind deconvolution algorithms," in *Proc. IEEE Conf. Comput. Vis. Pattern Recognit.*, 2009, pp. 1964–1971.

[10] S. Cho and S. Lee, "Fast motion deblurring," *Proc. ACM SIGGRAPH Asia*, vol. 28, no. 5, 2009, Art. no. 145.

[11] L. Xu and J. Jia, "Two-phase kernel estimation for robust motion deblurring," in *Proc. Eur. Conf. Comput. Vis.*, 2010, pp. 157–170.

[12] T. Michaeli and M. Irani, "Blind deblurring using internal patch recurrence," in *Proc. Eur. Conf. Comput. Vis.*, 2014, pp. 783–798.

[13] J. Pan, Z. Hu, Z. Su, and M.-H. Yang, "Deblurring face images with exemplars," in *Proc. Eur. Conf. Comput. Vis.*, 2014, pp. 47–62.

[14] X. Chen, X. He, J. Yang, and Q. Wu, "An effective document image deblurring algorithm," in *Proc. IEEE Conf. Comput. Vis. Pattern Recognit.*, 2011, pp. 369–376.

[15] H. Cho, J. Wang, and S. Lee, "Text image deblurring using text-specific properties," in *Proc. Eur. Conf. Comput. Vis.*, 2012, pp. 524–537.

[16] Z. Hu, S. Cho, J. Wang, and M.-H. Yang, "Deblurring low-light images with light streaks," in *Proc. IEEE Conf. Comput. Vis. Pattern Recognit.*, 2014, pp. 3382–3389.

[17] R. Köhler, M. Hirsch, B. J. Mohler, B. Schölkopf, and S. Harmeling, "Recording and playback of camera shake: Benchmarking blind deconvolution with a real-world database," in *Proc. Eur. Conf. Comput. Vis.*, 2012, pp. 27–40.

[18] L. Sun, S. Cho, J. Wang, and J. Hays, "Edge-based blur kernel estimation using patch priors," in *Proc. IEEE Int. Conf. Comput. Photography*, 2013, pp. 1–8.

[19] J. Pan, D. Sun, H. Pfister, and M.-H. Yang, "Blind image deblurring using dark channel prior," in *Proc. IEEE Conf. Comput. Vis. Pattern Recognit.*, 2016, pp. 1628–1636.

[20] J. Jia, *Mathematical Models and Practical Solvers for Uniform Motion Deblurring*. Cambridge, U.K.: Cambridge Univ. Press, 2014.

[21] J.-F. Cai, H. Ji, C. Liu, and Z. Shen, "Framelet based blind motion deblurring from a single image," *IEEE Trans. Image Process.*, vol. 21, no. 2, pp. 562–572, Feb. 2012.

[22] Y. Lou, A. L. Bertozzi, and S. Soatto, "Direct sparse deblurring," *J. Math. Imaging Vis.*, vol. 39, no. 1, pp. 1–12, 2011.

[23] H. Takeda, S. Farsiu, and P. Milanfar, "Deblurring using regularized locally adaptive kernel regression," *IEEE Trans. Image Process.*, vol. 17, no. 4, pp. 550–563, Apr. 2008.

[24] H. Zhang, J. Yang, Y. Zhang, and T. S. Huang, "Sparse representation based blind image deblurring," in *Proc. IEEE Int. Conf. Multimedia Expo*, 2011, pp. 1–6.

[25] D. Perrone and P. Favaro, "Total variation blind deconvolution: The devil is in the details," in *Proc. IEEE Conf. Comput. Vis. Pattern Recognit.*, 2014, pp. 2909–2916.

[26] N. Joshi, R. Szeliski, and D. J. Kriegman, "PSF estimation using sharp edge prediction," in *Proc. IEEE Conf. Comput. Vis. Pattern Recognit.*, 2008, pp. 1–8.

[27] Y. HaCohen, E. Shechtman, and D. Lischinski, "Deblurring by example using dense correspondence," in *Proc. Int. Conf. Comput. Vis.*, 2013, pp. 2384–2391.

[28] C. J. Schuler, M. Hirsch, S. Harmeling, and B. Schölkopf, "Learning to deblur," *IEEE Trans. Pattern Anal. Mach Intell.*, vol. 38, no. 7, pp. 1439–1451, July 2016.

[29] D. Zoran and Y. Weiss, "A neural approach to blind motion deblurring," in *Proc. Eur. Conf. Comput. Vis.*, 2016, pp. 221–235.

[30] J. Sun, W. Cao, Z. Xu, and J. Ponce, "Learning a convolutional neural network for non-uniform motion blur removal," in *Proc. IEEE Conf. Comput. Vis. Pattern Recognit.*, 2015, pp. 769–777.

[31] P. Wieschollek, B. Schölkopf, H. P. A. Lensch, and M. Hirsch, "End-to-end learning for image burst deblurring," in *Proc. Asian Conf. Comput. Vis.*, 2016, pp. 35–51.

[32] K. He, J. Sun, and X. Tang, "Single image haze removal using dark channel prior," in *Proc. IEEE Conf. Comput. Vis. Pattern Recognit.*, 2009, pp. 1956–1963.

[33] D. Martin, C. Fowlkes, D. Tal, and J. Malik, "A database of human segmented natural images and its application to evaluating segmentation algorithms and measuring ecological statistics," in *Proc. Int. Conf. Comput. Vis.*, 2001, pp. 416–423.

[34] L. Xu, C. Lu, Y. Xu, and J. Jia, "Image smoothing via L_0 gradient minimization," *ACM SIGGRAPH Asia*, vol. 30, no. 6, 2011, Art. no. 174.

[35] J. Tang, et al., "Tri-clustered tensor completion for social-aware image tag refinement," *IEEE Trans. Pattern Anal. Mach. Intell.*, vol. 39, no. 8, pp. 1662–1674, Aug. 2017.

[36] Y. Wang, J. Yang, W. Yin, and Y. Zhang, "A new alternating minimization algorithm for total variation image reconstruction," *SIAM J. Imaging Sci.*, vol. 1, no. 3, pp. 248–272, 2008.

[37] J. Pan, Z. Hu, Z. Su, and M.-H. Yang, "L_0-regularized intensity and gradient prior for deblurring text images and beyond," *IEEE Trans. Pattern Anal. Mach. Intell.*, vol. 39, no. 2, pp. 342–355, Feb. 2017.

[38] A. Gupta, N. Joshi, C. L. Zitnick, M. F. Cohen, and B. Curless, "Single image deblurring using motion density functions," in *Proc. Eur. Conf. Comput. Vis.*, 2010, pp. 171–184.

[39] M. Hirsch, C. J. Schuler, S. Harmeling, and B. Schölkopf, "Fast removal of non-uniform camera shake," in *Proc. IEEE Int. Conf. Comput. Vis.*, 2011, pp. 463–470.

[40] Q. Shan, W. Xiong, and J. Jia, "Rotational motion deblurring of a rigid object from a single image," in *Proc. IEEE Int. Conf. Comput. Vis.*, 2007, pp. 1–8.

[41] Y.-W. Tai, P. Tan, and M. S. Brown, "Richardson-Lucy deblurring for scenes under a projective motion path," *IEEE Trans. Pattern Anal. Mach. Intell.*, vol. 33, no. 8, pp. 1603–1618, Aug. 2011.

[42] O. Whyte, J. Sivic, A. Zisserman, and J. Ponce, "Non-uniform deblurring for shaken images," *Int. J. Comput. Vis.*, vol. 98, no. 2, pp. 168–186, 2012.

[43] D. Zoran and Y. Weiss, "From learning models of natural image patches to whole image restoration," in *Proc. IEEE Int. Conf. Comput. Vis.*, 2011, pp. 479–486.

[44] D. Perrone and P. Favaro, "A logarithmic image prior for blind deconvolution," *Int. J. Comput. Vis.*, vol. 117, no. 2, pp. 159–172, 2016.

[45] L. Xiao, J. Wang, W. Heidrich, and M. Hirsch, "Learning high-order filters for efficient blind deconvolution of document photographs," in *Proc. Eur. Conf. Comput. Vis.*, 2016, pp. 734–749.

[46] J. Pan, Z. Lin, Z. Su, and M.-H. Yang, "Robust kernel estimation with outliers handling for image deblurring," in *Proc. IEEE Conf. Comput. Vis. Pattern Recognit.*, 2016, pp. 2800–2808.

[47] S. Cho, J. Wang, and S. Lee, "Handling outliers in non-blind image deconvolution," in *Proc. IEEE Int. Conf. Comput. Vis.*, 2011, pp. 495–502.

[48] Z. Hu and M.-H. Yang, "Good regions to deblur," in *Proc. Eur. Conf. Comput. Vis.*, 2012, pp. 59–72.

[49] D. Lemire, "Streaming maximum-minimum filter using no more than three comparisons per element," *Nordic J. Comput.*, vol. 13, no. 4, pp. 328–339, 2006.

[50] C. Chen, M. N. Do, and J. Wang, "Robust image and video dehazing with visual artifact suppression via gradient residual minimization," in *Proc. Eur. Conf. Comput. Vis.*, 2016, pp. 576–591.

Jinshan Pan received the PhD degree in computational mathematics from Dalian University of Technology, China, in 2017. He was a joint-training PhD student in School of Mathematical Sciences at and Electrical Engineering and Computer Science, University of California, Merced, California from 2014 to 2016. He is a professor of the School of Computer Science and Engineering, Nanjing University of Science and Technology. His research interests include image deblurring, image/video analysis and enhancement, and related vision problems.
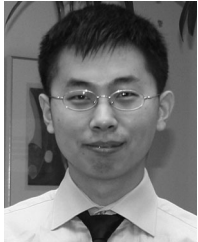
Deqing Sun received the BEng degree in electronic and information engineering from Harbin Institute of Technology, the MPhil degree in electronic engineering from Chinese University of Hong Kong, and the MS and PhD degrees in computer science from Brown University. He is a senior research scientist with NVIDIA Research. He was a research intern with Microsoft Research New England from October to December 2010. He was a postdoctoral fellow with Harvard University before joining NVIDIA Research. His research interests include computer vision, machine learning and signal processing, particularly optical flow estimation, motion segmentation and their applications to video processing. He is a member of the IEEE.

Hanspeter Pfister received the MS degree in electrical engineering from ETH Zurich, Switzerland and the PhD degree in computer science from State University of New York at Stony Brook. He is an wang professor of computer science in the School of Engineering and Applied Sciences, Harvard University. He is director of the Institute for Applied Computational Science. Before joining Harvard, he worked for over a decade with Mitsubishi Electric Research Laboratories where he was associate director and senior research scientist. He was the chief architect of VolumePro, Mitsubishi Electric's award-winning real-time volume rendering hardware for PCs. He is the recipient of the 2010 IEEE Visualization Technical Achievement award and the Petra T. Shattuck Excellence in Teaching Award in 2009. He is co-editor of the first textbook on Point-Based Computer Graphics, published by Elsevier in 2007, and was Technical Papers Chair for SIGGRAPH 2012.

Ming-Hsuan Yang received the PhD degree in computer science from the University of Illinois at Urbana-Champaign, in 2000. He is a professor of electrical engineering and computer science with the University of California, Merced. He served as an associate editor of the *IEEE Transactions on Pattern Analysis and Machine Intelligence* from 2007 to 2011, and is an associate editor of the *International Journal of Computer Vision, Image and Vision Computing*, and the *Journal of Artificial Intelligence Research*. He received the NSF CAREER Award in 2012, and the Google Faculty Award in 2009. He is a senior member of the IEEE and the ACM.

▷ **For more information on this or any other computing topic, please visit our Digital Library at** www.computer.org/publications/dlib.